Applied Physics Letters

Ultra-wide-bandgap AlGaN homojunction tunnel diodes with negative differential resistance

Cite as: Appl. Phys. Lett. **115**, 082104 (2019); https://doi.org/10.1063/1.5113503
Submitted: 04 June 2019 . Accepted: 06 August 2019 . Published Online: 21 August 2019

Evan A. Clinton, Zachary Engel, Ehsan Vadiee, Joe V. Carpenter, Zachary C. Holman, and W. Alan Doolittle

AIP Publishing

Applied Physics Letters ARTICLE scitation.org/journal/apl

Ultra-wide-bandgap AlGaN homojunction tunnel diodes with negative differential resistance

Cite as: Appl. Phys. Lett. **115**, 082104 (2019); doi: 10.1063/1.5113503
Submitted: 4 June 2019 · Accepted: 6 August 2019 ·
Published Online: 21 August 2019

Evan A. Clinton,[1] Zachary Engel,[1] Ehsan Vadiee,[1] Joe V. Carpenter,[2] Zachary C. Holman,[2] and W. Alan Doolittle[1,a)]

AFFILIATIONS

[1]School of Electrical and Computer Engineering, Georgia Institute of Technology, Atlanta, Georgia 30332, USA
[2]School of Electrical, Computer, and Energy Engineering, Arizona State University, Tempe, Arizona 85287, USA

[a)]Author to whom correspondence should be addressed: alan.doolittle@ece.gatech.edu

ABSTRACT

The power efficiencies of state-of-the-art $Al_xGa_{1-x}N$ deep-ultraviolet (UV) emitters operating in the <300 nm wavelength region are currently limited to a few percent in part due to limitations in the series and contact resistance which result in excessive drive voltages. $Al_xGa_{1-x}N$ tunnel contacts and tunnel junctions in deep-UV devices are a promising route toward increasing these efficiencies by improving the contact resistances, hole injection, and reducing optical absorption by removing undesirable p-GaN contact layers. However, due to doping inefficiencies, standalone tunnel diodes have not been realized in the form of homojunction $Al_xGa_{1-x}N$. In this work, $Al_xGa_{1-x}N$ ($0.19 \leq x \leq 0.58$) homojunction tunnel diodes are fabricated with high reverse bias current densities, and one device with $x = 0.19$ demonstrates a negative differential resistance at ~2.4 V. $Al_xGa_{1-x}N$ p++/n++/n tunnel diodes are compared to reference p++/i/n diodes to provide clarity about the role of tunneling conduction vs leakage conduction. Transmission electron microscopy verifies that heavy doping does not result in visible defects such as Mg precipitates and allows for subsequent epitaxy, critical for buried tunnel junction structures. Increasing the bandgap energy of $Al_xGa_{1-x}N$ for higher Al content tunnel junctions decreases the tunnel current, but still allows sufficient conduction necessary for future improvements in deep UV emitter efficiencies.

AlGaN-based ultraviolet (UV) emitters, light-emitting diodes (LEDs), and lasers, have a broad range of applications, such as water and air purification, medical sterilization, and biochemistry.[1] However, the external quantum efficiency of AlGaN-based UV emitters dramatically reduces when reducing the emission wavelength further into the deep UV due to multiple growth and fabrication issues.[2] The low efficiencies and weak light extraction of AlGaN-based UV LEDs mainly stem from the high threading dislocation densities, high UV absorption coefficients, poor hole injection of p-GaN layers, and high resistance of p-GaN contact layers.[2–4]

Generally, as the bandgap and Al composition increase, the AlGaN film suffers from elevated defect densities, and increased ionization energies of dopants for both n- and p-type AlGaN (with different rates). The latter issue contributes to asymmetric carrier injection into the active region of LEDs (e.g., lack of efficient hole injection), which causes electron leakage out of the active region. It is reported that among all causes of efficiency droop in LEDs, such as Auger recombination and defect-assisted Shockley-Read-Hall (SRH) recombination, insufficient hole injection is the key loss mechanism.[5–7] The hole injection issue can be dramatically improved by forming a homojunction tunnel junction (TJ), in which a transparent n-AlGaN top tunnel contact (TC) layer can be connected to the p-AlGaN contact layer to improve light extraction and eliminate the need for flip-chip bonding. The use of an AlGaN TC instead of p-GaN leads to the reduction of parasitic optical absorption in the p-GaN contact layer while also providing high hole current with an ideally low turn-on voltage penalty resulting from the additional junction. In addition, AlGaN TJs can be connected to p-AlGaN cladding layers in edge-emitting lasers and n-type distributed Bragg reflectors in vertical-cavity surface-emitting lasers (VCSELs).

III-nitride-based TJs have been studied to series-connect devices, to reduce device fabrication steps (e.g., combining n- and p-type contact patterning and metallization), but primarily as n-type TCs to p-type layers to substantially reduce contact resistance by orders of magnitude.[8–10] Low-resistance polarization engineered TJs have been demonstrated to enhance tunneling probabilities (e.g., for GaN by inserting an interlayer typically InGaN or AlN).[11] Nevertheless, the use of a heterojunction interlayer introduces material degradation due to lattice

mismatch and parasitic light absorption. Furthermore, heterojunction TJs become increasingly more problematic as the AlGaN bandgap is increased. With higher Al compositions, a change in piezoelectric properties needed to form a polarization engineered junction is difficult without significant changes in the Al composition, and with higher growth temperatures is less practical by adding In.

Recently, GaN homojunction tunnel diodes (TDs) with a negative differential resistance (NDR) and tunnel contacts to p/i/n devices have been introduced using plasma-assisted molecular beam epitaxy (PAMBE) with voltage penalties as low as 0.1 V.[9] The NDR in forward bias in these devices is suspected to be from defect-assisted tunneling and not from Esaki-style band-to-band tunneling. Although the tunneling mechanism is defect-assisted, the extreme n- and p-type doping is still required to narrow the depletion width enough to enable any defect-assisted tunneling in forward bias. GaN-based homojunction and heterojunction TJs have been integrated into optoelectronic devices, such as LEDs,[12] solar cells,[10] vertical-cavity surface-emitting lasers (VCSELs),[13] and cascade LEDs.[8] However, achieving a low-resistance TJ for wide-bandgap AlGaN materials is extremely challenging because of the high depletion widths (due to low doping concentrations in AlGaN) and large barrier heights (related to the bandgap of AlGaN). AlGaN homojunction TJs for UV optoelectronics are particularly difficult with traditional growth techniques such as metal-organic chemical vapor deposition (MOCVD) and MBE, where p-type doping is insufficiently low. Recently, polarization engineered TJs using AlGaN/GaN structures have been reported exhibiting low tunneling resistances of $9.4 \times 10^{-4}\,\Omega\,\mathrm{cm}^2$ at $1.0\,\mathrm{kA/cm}^2$ for a tunnel-contacted UV-LED operating at 292 nm.[14,15] Similar to GaN, the aforementioned polarization engineered TJ can generate defects, light absorption, and growth complications. In this work, we demonstrate standalone heavily doped AlGaN p++/n++ homojunction TDs with NDR up to 19% Al and reverse bias tunneling characteristics up to 58% Al.

To achieve tunneling in homojunction AlGaN TJs, it is necessary to achieve both heavily doped n- and p-type films at high Al compositions. It has been reported that using silicon as an n-type dopant for $Al_xGa_{1-x}N$ is more favorable than germanium.[16] Silicon doping of $Al_xGa_{1-x}N$ in an MOCVD reactor has been reported up to $x = 1$, but the ionization energy was measured to increase from ~8 (GaN) to 86 meV (AlN).[17] p-type doping remains problematic for all III-N-based materials when employing traditional growth techniques, such as MOCVD or MBE. For MOCVD, the activation energy increases from ~170 meV for GaN to 510 meV for AlN.[18]

In this work, the metal-modulated epitaxy (MME) growth technique at low temperatures (<720 °C) in a PAMBE chamber is implemented. MME has been reported to achieve hole concentrations up to $7 \times 10^{19}\,\mathrm{cm}^{-3}$ for GaN and a lower activation energy down to 43 meV.[19] Additionally, a hole concentration of $2.3 \times 10^{19}\,\mathrm{cm}^{-3}$ for an $Al_{0.27}Ga_{0.73}N$ film was reported using the MME growth technique.[20] Such extreme p-type doping of AlGaN is likely due to a combination of the lower growth substrate temperature employed and the shuttered MME technique, which may allow Mg atoms to stick and more effectively incorporate under favorable surface chemistry to minimize compensating defects.[21] Although the growth substrate temperature is low, the metal adlayer in the MME technique enables large adatom diffusion lengths, and the films maintain smooth surface morphologies.[22] With this hydrogen-free technique and more traditional MBE, the Mg atoms are activated as-grown without an activation annealing step that is common for MOCVD growth of p-GaN.[23] The MOCVD annealing step is required to allow for hydrogen out-diffusion from the material and is difficult for buried p-type layers unless they are of a suitably small geometry to allow lateral diffusion out from the sidewalls.[24] The low-temperature MME growth technique enables high hole concentrations as well as device design flexibility with buried p-type layers as-grown, without an anneal.

First, to explore the effect of increasing Al content on the resistivity and electron concentration of the n- and p-AlGaN films, three 100 nm-thick n-type and three p-type AlGaN calibration samples were grown with Al compositions up to ~60% via MME on AlN buffer layers grown on AlN templates (threading dislocation density $\sim 2 \times 10^9\,\mathrm{cm}^{-3}$ obtained from Sandia National Laboratories, NM, USA) at growth temperatures between 680 and 720 °C (depending on the Al composition).

The n-AlGaN films were grown with a silicon flux ($[\mathrm{Si}] = 1.9 \times 10^{20}\,\mathrm{cm}^{-3}$ for GaN calibrations). Figure 1 illustrates that with increasing Al composition, the van-der Pauw resistivity increases by a factor of 83 from 3.5×10^{-4} to $2.9 \times 10^{-2}\,\Omega\,\mathrm{cm}$, while the Hall electron concentration only decreases by a factor of 4.8 from 1.8×10^{20} to $3.8 \times 10^{19}\,\mathrm{cm}^{-3}$. The reduction in the electron concentration is likely due to the increase in the dopant activation energy.[16] The mismatch in the rate of increasing resistivity with the rate of decreasing electron concentration is the result of elevated alloy disorder scattering or defect scattering for higher Al content films.

The p-AlGaN films were grown with a constant flux of magnesium ($[\mathrm{Mg}] = 5.3 \times 10^{20}\,\mathrm{cm}^{-3}$ for GaN). The room-temperature Hall hole concentrations were not compared for the p-AlGaN films because they were unmeasurable with the Hall effect due to a low strength fixed magnet of 0.3 T, but clearly showed p-type conduction in thermal probe measurements. Given that p-GaN films with this excessively high doping are already near the lower limit of Hall mobility measurement capability, it is not surprising that the heavily doped random alloy is unmeasurable. As seen in Fig. 1(a), the p-type films exhibit a large (~730×) increase in the van-der Pauw resistivity from $2.6 \times 10^{-1}\,\Omega\,\mathrm{cm}$ for p-GaN to $1.9 \times 10^{2}\,\Omega\,\mathrm{cm}$ for $p\text{-}Al_{0.64}Ga_{0.36}N$. The resistivity of the n- and p-AlGaN films with high Al compositions resulted in higher resistances and reduced doping concentrations, which will increase the depletion widths for AlGaN TJs and significantly decrease the tunneling probability.

In order to investigate tunneling in AlGaN devices, three heavily doped p++/n++/n AlGaN homojunction TDs (B1, B2, and B3) were grown at Al compositions of ~19%, 42%, and 58%, respectively, and

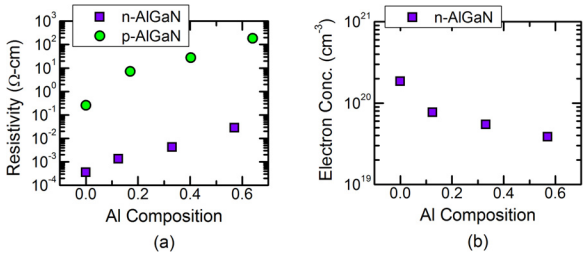

FIG. 1. Effect of Al composition on (a) van-der Pauw resistivity of n- and p-AlGaN films and (b) Hall electron concentration of n-AlGaN films (p-AlGaN hole concentrations were unmeasurable for the Hall effect with a fixed magnet of 0.3 T, but clearly showed p-type conduction in thermal probe measurements).

are shown in Fig. 2(b). Since increased conduction can be attributed to either the fundamental tunneling mechanisms or merely leakage current, three AlGaN p++/i/n control diodes (A1–A3) were grown at similar Al contents and are compared to the p++/n++/n TDs and are shown in Fig. 2(a). The depletion widths in the control diodes with the 50 nm intrinsic layers are sufficiently wide to prevent tunneling, while the heavy doping in structure B significantly decreases the depletion widths to promote tunneling.

Growth of both structure A and B was initiated by 100 nm of unintentionally doped AlN buffer layers on AlN templates. An AlN template was chosen to electrically isolate the template from the homojunction devices, and to ensure that the films are either relaxed or compressively strained to prevent material degradation or cracking. The 130 nm lower n- and 50 nm top p-type layer dopant concentrations in both structures were $[Si] = 1.9 \times 10^{20}\,cm^{-3}$ and $[Mg] = 5.3 \times 10^{20}\,cm^{-3}$, respectively. These dopant concentrations are the same as those used in the calibration samples, shown in Fig. 1, but with slightly different Al compositions of 19%, 42%, and 58%, which are within the calibrated range. Structure B contains an additional heavily doped n-type layer (instead of the i-layer in structure A) with a concentration of $[Si] = 4.60 \times 10^{20}\,cm^{-3}$ to form a TJ at the p++/n++ interface.

The growth temperature was changed depending on the Al composition. The growth temperature was set to 680, 700, and 720 °C for the Al compositions of 19%, 42%, and 58%, respectively. Atomic force microscopy (not shown here) confirmed that a two-dimensional growth mode was maintained and demonstrated RMS roughness values of ~1–2 nm.

Samples A1–A3 and B1–B3 shown in Fig. 2 were fabricated into 200 μm circular mesa devices using standard photolithography and an inductively coupled plasma (ICP) etching procedure with BCl_3 and Cl_2 gases to define the mesa structure. A metal stack of Ti(300 Å)/Al(1000 Å)/Ti(300 Å)/Au(500 Å) and Pt(50 Å)/Pd(50 Å)/Au(500 Å) was deposited using e-beam evaporation for n- and p-type contacts, respectively. The contacts were not annealed in this study, because the heavily Mg-doped layers behave differently when annealed.[25] These results are similar to our previous work with GaN, where the heavy doping and activated, as-grown n- and p-type layers enabled Ohmic conduction.[9]

The semilog current-voltage characteristics for A1–A3 and B1–B3 are presented in Fig. 3. Device B1, shown in Fig. 3(a), exhibits

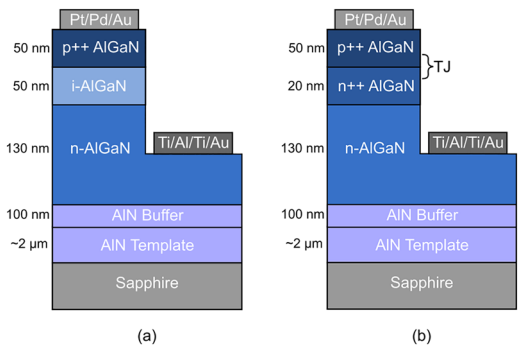

FIG. 2. AlGaN homojunction device structures for (a) p++/i/n (structure A) and (b) p++/n++/n (structure B) devices.

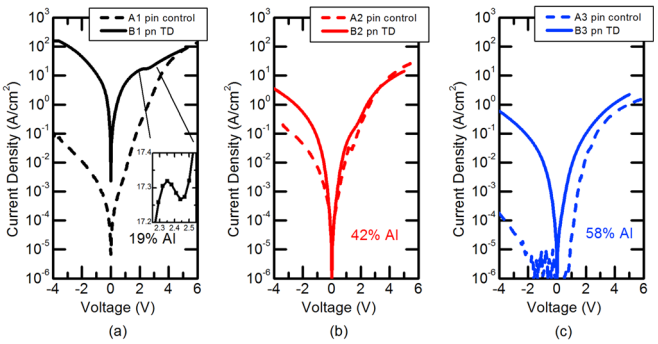

FIG. 3. Semilog current-voltage characteristics for p++/i/n control and p++/n++ tunnel diode devices (a) A1 and B1 (inset: linear NDR for B1), (b) A2 and B2, and (c) A3 and B3. A negative differential resistance is present in sample B1. High reverse bias conductivities are observed for B1–B3 when compared to their control diodes A1–A3.

NDR in forward bias with a low peak-to-valley current ratio (PVCR) of ~1.003 at a peak voltage of 2.35 V, slightly lower than those of previously reported in homojunction GaN TDs (PVCR of 1.01 to 1.1).[9,26] The ideality factor (n) for B1 is much greater than two, which is common in nitride-based devices, especially those grown on inexpensive sapphire substrates. Homoepitaxially grown GaN devices on bulk GaN substrates with low dislocation densities have been demonstrated to achieve a record low $n = 1.1$.[27] The high peak voltage and ideality factor $n \gg 2$ further suggest a defect-assisted tunneling mechanism and not Esaki-style band-to-band tunneling. For band-to-band tunneling in forward bias, the peak voltage is related to the degenerate doping on both sides of the junction and would take place at low voltages (e.g., <0.4 V).[28]

Samples B1–B3 display asymmetric current density profiles. The current densities of samples B1–B3 at −1.0 V are 118%, 68%, and 49% higher than those at 1.0 V. The increased conductivity in reverse bias indicates tunneling via a narrowed depletion width, and the tunneling reduces with an increasing Al content, as previously discussed due to the wider depletion widths resulting from lower dopant concentrations at an elevated Al content. The control diodes A1–A3 do not exhibit tunneling, as expected. The current-voltage characteristics of diodes A1–A3 represent more traditional rectification, but they do have higher than predicted reverse-bias leakage currents, especially for A1 and A2, likely due to thin intrinsic layers and the presence of defects in the heteroepitaxial growth performed here (see later discussion). When comparing the current densities at a reverse bias of −4.0 V of the control devices to the tunnel devices, both the lowest and highest Al content pairs of samples [A1 to B1 in Fig. 3(a), and A3 to B3 in Fig. 3(c)] exhibit an increase in almost four orders of magnitude indicating tunnel conduction is indeed the responsible mechanism, and not merely leakage current. Thus, by separating the n++ and p++ regions by 50 nm, which is beyond the tunneling length, tunneling is suppressed in the control structure. Additionally, each pair of structures (e.g., A1 and B1) has a similar current density at higher forward biases when thermionic emission begins to dominate, and tunneling is negligible.

In order to verify that tunneling was not a result of poor structural quality (e.g., phase separation, pits, cracking), the samples B1-B3

were measured via x-ray diffraction (XRD) and scanning transmission electron microscopy (STEM) techniques. The XRD asymmetric $(10\bar{1}5)$ reciprocal space maps (RSMs) are displayed in Fig. 4. The films are single composition and partially relaxed. The films may have an initial thin layer that is more strained to the template, and once the critical thickness is exceeded, a more relaxed layer forms, similar to $In_xGa_{1-x}N$/GaN films.[29–31] The films' $(10\bar{1}5)$ omega rocking curve FWHM values increase from 842 to 1459 arcsecs for B1 to B3, while the (0002) FWHM decreases from 634 to 487 arcsecs. The trend of FWHM values indicates that at a higher Al content, the films are slightly more columnar, similar to previous findings for GaN.[32] This columnar effect may be mitigated in the future with a more optimized MME condition and thicker buffer layers.

STEM images of sample B1 were taken using a JEOL ARM200F operated at 200 keV, and are displayed in Fig. 5. The entire structure is shown in Fig. 5(a). It is well known that AlN surfaces contain adsorbed oxygen that is notoriously difficult to remove. It appears that the unoptimized nucleation of the MME AlN buffer layer on the AlN template contains many defects (e.g., oxygen) that generate dislocations which propagate through the buffer and into the AlGaN layers, a well-known issue.[33] Figure 5(b) is a high-resolution image at the TJ p++/n++ interface representing the overall images found for this device. Figure 5(b) does not indicate Mg precipitates or visible defects related to the extreme doping, but they may still be present in other regions of the device not imaged. Due to the lack of extended defects associated with doping, point defects which cannot be observed with STEM are likely the source of the defect-assisted tunneling.

The ability to heavily dope AlGaN layers while allowing high-quality subsequent epitaxy is promising for devices with buried TJs, such as series-connected LEDs, or tunnel-contacted p-down structures but will require a process for sufficient removal of oxygen contamination from the AlN templates.

In conclusion, the low-temperature MME growth technique is employed to achieve single-phase, heavily doped AlGaN layers. The doping is progressively more difficult at high Al compositions, where the activation efficiency of dopants reduces and where the low-temperature growth technique is less optimal, and defect formation occurs. However, AlGaN homojunction TDs have been fabricated and are compared to control diodes to investigate the Al compositional limits of tunneling. A forward bias NDR is observed up to $x = 0.19$, indicating a narrow depletion width, and thus extreme dopant concentrations. Reverse bias tunneling is observed for all devices up to 58% Al, but the magnitude of the tunneling current decreases with the increasing Al content. The low-temperature MME growth technique presented here and applied to AlGaN TJs enables alternatives to unfavorable p-GaN layers and may enable future improved hole injection and power efficiency for deep UV emitters.

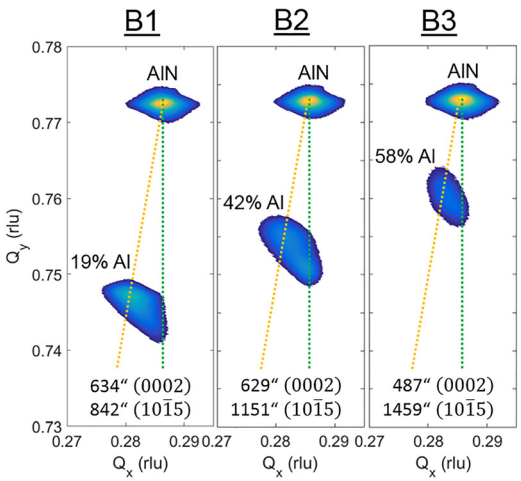

FIG. 4. XRD $(10\bar{1}5)$ RSMs for samples B1–B3. The AlN template location, the $Al_xGa_{1-x}N$ film's location and associated Al content, and the measured (0002)and $(10\bar{1}5)$ FWHM values are all labeled. The vertical (green) and diagonal (orange) dashed lines correspond to the fully strained and full-relaxed film positions, respectively.

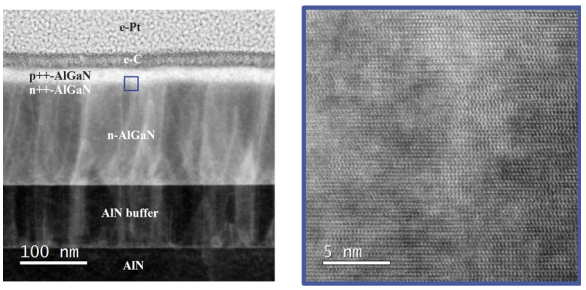

FIG. 5. Scanning transmission electron microscopy of sample B1: (a) entire structure and (b) the p++/n++ TJ interface (the highlighted region in (a)) shows no significant structural degradation.

This work was supported in part by the National Science Foundation (NSF) and the Department of Energy under Nos. NSF CA EEC-1041895 and NSF SG DMR-1710032 and in part by the Advanced Research Projects Agency-Energy, U.S. Department of Energy, under Award No. DEAR0000470. The authors would also like to acknowledge Dr. Brendan Gunning at Sandia National Laboratories for supplying the AlN templates.

REFERENCES

[1]M. A. Khan, Phys. Status Solidi **203**, 1764 (2006).
[2]H. Hirayama, N. Maeda, S. Fujikawa, S. Toyoda, and N. Kamata, Jpn. J. Appl. Phys., Part 1 **53**, 100209 (2014).
[3]H. Ryu, I. Choi, H. H. R. I. Choi, J. Shim, and H. C. J. Shim, Appl. Phys. Express **6**, 062101 (2013).
[4]N. Maeda and H. Hirayama, Phys. Status Solidi **10**, 1521 (2013).
[5]J. Cho, E. F. Schubert, and J. K. Kim, Laser Photonics Rev. **7**, 408 (2013).
[6]Q. Dai, Q. Shan, J. Wang, S. Chhajed, J. Cho, E. F. Schubert, M. H. Crawford, D. D. Koleske, M.-H. Kim, and Y. Park, Appl. Phys. Lett. **97**, 133507 (2010).
[7]E. Kioupakis, P. Rinke, K. T. Delaney, and C. G. Van De Walle, Appl. Phys. Lett. **98**, 161107 (2011).
[8]M. J. Grundmann and U. K. Mishra, Phys. Status Solidi **4**, 2830 (2007).
[9]E. A. Clinton, E. Vadiee, S. C. Shen, K. Mehta, P. D. Yoder, and W. A. Doolittle, Appl. Phys. Lett. **112**, 252103 (2018).
[10]E. Vadiee, E. A. Clinton, H. McFavilen, A. S. Weidenbach, Z. Engel, C. Matthews, C. Zhang, C. Arena, R. R. King, C. B. Honsberg, and W. A. Doolittle, Appl. Phys. Express **11**, 082304 (2018).
[11]D. Jena, J. Simon, A. K. Wang, Y. Cao, K. Goodman, J. Verma, S. Ganguly, G. Li, K. Karda, V. Protasenko, C. Lian, T. Kosel, P. Fay, and H. Xing, Phys. Status Solidi **208**, 1511 (2011).

[12]Z. H. Zhang, S. T. Tan, Z. Kyaw, Y. Ji, W. Liu, Z. Ju, N. Hasanov, X. W. Sun, and H. V. Demir, Appl. Phys. Lett. **102**, 193508 (2013).
[13]S. Lee, C. A. Forman, C. Lee, J. Kearns, E. C. Young, J. T. Leonard, D. A. Cohen, J. S. Speck, S. Nakamura, and S. P. Denbaars, Appl. Phys. Express **11**, 062703 (2018).
[14]Y. Zhang, S. Krishnamoorthy, F. Akyol, A. A. Allerman, M. W. Moseley, M. Armstrong, and S. Rajan, Appl. Phys. Lett. **109**, 121102 (2016).
[15]Y. Zhang, S. Krishnamoorthy, J. M. Johnson, F. Akyol, A. Allerman, M. W. Moseley, A. Armstrong, and J. Hwang, Appl. Phys. Lett. **106**, 141103 (2015).
[16]P. Bogusławski and J. Bernholc, Phys. Rev. B **56**, 9496 (1997).
[17]Y. Taniyasu, M. Kasu, and N. Kobayashi, Appl. Phys. Lett. **81**, 1255 (2002).
[18]K. B. Nam, M. L. Nakarmi, J. Li, J. Y. Lin, and H. X. Jiang, Appl. Phys. Lett. **83**, 878 (2003).
[19]B. Gunning, J. Lowder, M. Moseley, W. A. Doolittle, and W. Alan Doolittle, Appl. Phys. Lett. **101**, 082106 (2012).
[20]B. P. Gunning, C. A. M. Fabien, J. J. Merola, E. A. Clinton, W. A. Doolittle, S. Wang, A. M. Fischer, and F. A. Ponce, J. Appl. Phys. **117**, 045710 (2015).
[21]A. Pandey, X. Liu, Z. Deng, W. J. Shin, D. A. Laleyan, K. Mashooq, E. T. Reid, E. Kioupakis, P. Bhattacharya, and Z. Mi, Phys. Rev. Mater. **3**, 053401 (2019).
[22]M. Moseley, D. Billingsley, W. Henderson, E. Trybus, and W. A. Doolittle, J. Appl. Phys. **106**, 014905 (2009).
[23]S. Nakamura, T. Mukai, M. Senoh, I. Naruhito, and N. Iwasa, Jpn. J. Appl. Phys., Part 2 **31**, L 139 (1992).
[24]Y. Kuwano, M. Kaga, T. Morita, K. Yamashita, K. Yagi, M. Iwaya, T. Takeuchi, S. Kamiyama, and I. Akasaki, Jpn. J. Appl. Phys., Part 1 **52**, 08JK12 (2013).
[25]M. E. Zvanut, Y. Uprety, J. Dashdorj, M. Moseley, and W. Alan Doolittle, J. Appl. Phys. **110**, 044508 (2011).
[26]F. Akyol, S. Krishnamoorthy, Y. Zhang, J. Johnson, J. Hwang, and S. Rajan, Appl. Phys. Lett. **108**, 131103 (2016).
[27]Z. Hu, K. Nomoto, B. Song, M. Zhu, M. Qi, M. Pan, X. Gao, V. Protasenko, D. Jena, and H. G. Xing, Appl. Phys. Lett. **107**, 243501 (2015).
[28]L. Esaki, Phys. Rev. **109**, 603 (1958).
[29]E. A. Clinton, E. Vadiee, C. A. M. Fabien, M. W. Moseley, B. P. Gunning, W. A. Doolittle, A. M. Fischer, Y. O. Wei, H. Xie, and F. A. Ponce, Solid State Electron. **136**, 3 (2017).
[30]C. A. M. Fabien, B. P. Gunning, W. Alan Doolittle, A. M. Fischer, Y. O. Wei, H. Xie, and F. A. Ponce, J. Cryst. Growth **425**, 115 (2015).
[31]S. Pereira, M. R. Correia, E. Pereira, C. Trager-Cowan, F. Sweeney, K. P. O'Donnell, E. Alves, N. Franco, and A. D. Sequeira, Appl. Phys. Lett. **81**, 1207 (2002).
[32]B. Heying, X. H. Wu, S. Keller, Y. Li, D. Kapolnek, B. P. Keller, S. P. DenBaars, and J. S. Speck, Appl. Phys. Lett. **68**, 643 (1996).
[33]R. Dalmau, B. Moody, R. Schlesser, S. Mita, J. Xie, M. Feneberg, B. Neuschl, K. Thonke, R. Collazo, A. Rice, J. Tweedie, and Z. Sitar, J. Electrochem. Soc. **158**, H530 (2011).